

RE-ALIGN: Aligning Vision Language Models via Retrieval-Augmented Direct Preference Optimization

Anonymous ACL submission

Abstract

The emergence of large Vision Language Models (VLMs) has broadened the scope and capabilities of single-modal Large Language Models (LLMs) by integrating visual modalities, thereby unlocking transformative cross-modal applications in a variety of real-world scenarios. Despite their impressive performance, VLMs are prone to significant hallucinations, particularly in the form of cross-modal inconsistencies. Building on the success of Reinforcement Learning from Human Feedback (RLHF) in aligning LLMs, recent advancements have focused on applying direct preference optimization (DPO) on carefully curated datasets to mitigate these issues. Yet, such approaches typically introduce preference signals in a brute-force manner, neglecting the crucial role of visual information in the alignment process. In this paper, we introduce RE-ALIGN, a novel alignment framework that leverages image retrieval to construct a dual-preference dataset, effectively incorporating both textual and visual preference signals. We further introduce rDPO, an extension of the standard direct preference optimization that incorporates an additional visual preference objective during fine-tuning. Our experimental results demonstrate that RE-ALIGN not only mitigates hallucinations more effectively than previous methods but also yields significant performance gains in general visual question-answering (VQA) tasks. Moreover, we show that RE-ALIGN maintains robustness and scalability across a wide range of VLM sizes and architectures. This work represents a significant step forward in aligning multimodal LLMs, paving the way for more reliable and effective cross-modal applications.

1 Introduction

The recent emergence of powerful Vision Language Models (VLMs) (Li et al., 2022, 2023a; Liu et al., 2024a; Li et al., 2024b; Meta, 2024; Bai et al., 2023; Wang et al., 2024b; Lu et al., 2024; Wu et al.,

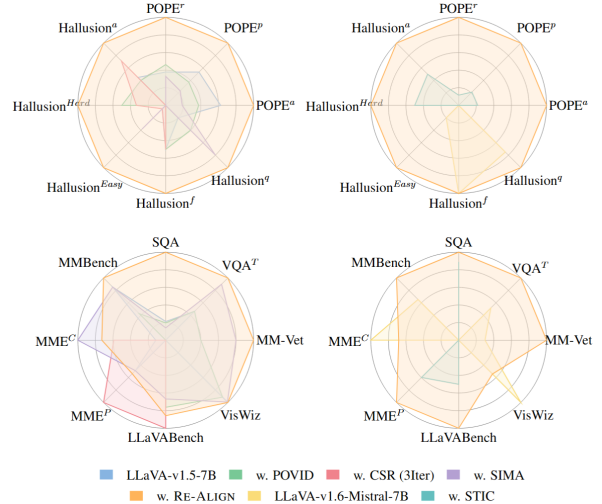


Figure 1: Benchmark performance comparison (min-max normalized).

2024) has significantly extended the capabilities of Large Language Models (LLMs) (Devlin et al., 2018; Radford et al., 2019; Brown et al., 2020; Team et al., 2023; Roziere et al., 2023; Touvron et al., 2023a,b; Raffel et al., 2020; Yang et al., 2024; Team, 2024) into the visual domain, paving the way for innovative real-world applications that integrate multimodal information (Moor et al., 2023; Li et al., 2024a; Shao et al., 2024; Xing et al., 2024b; Rana et al., 2023; Kim et al., 2024). Despite their promising performance, VLMs remain susceptible to hallucinations—instances where the model produces outputs containing inaccurate or fabricated details about objects, attributes, and the logical relationships inherent in the input image (Rohrbach et al., 2018; Bai et al., 2024). Several factors contribute to this cross-modal inconsistency, including the separate low-quality or biased training data, imbalanced model architectures, and the disjoint pretraining of the vision encoder and LLM-backbone (Cui et al., 2023; Bai et al., 2024; Zhou et al., 2024a).

To mitigate the hallucinations in VLMs, the Directed Preference Optimization (DPO) techniques have been widely adopted (Deng et al., 2024; Zhou

et al., 2024a; Fang et al., 2024; Zhou et al., 2024b; Guo et al., 2024; Chen et al., 2024; Wang et al., 2024c; Yu et al., 2024b; Li et al., 2023b; Wang et al., 2024a; Xiao et al., 2025; Xie et al., 2024; Fu et al., 2024). This involves constructing datasets enriched with human preference signals specifically targeting hallucinations, and then finetuning the models using algorithms like Direct Preference Optimization (DPO) (Rafailov et al., 2024). Existing methods generate the preference data by perturbing the ground truth responses (Zhou et al., 2024a) and corrupting the visual inputs/embeddings (Deng et al., 2024; Amirloo et al., 2024) to generate rejected responses or correcting/refining responses to produce chosen responses (Chen et al., 2024; Yu et al., 2023a). While methods based on response refinement yield the most reliable preference signals, they face scalability challenges due to the significant costs of manual correction processes. Conversely, directly corrupting input visual information or ground truth responses is overly simplistic, as this brute-force approach fails to generate plausible and natural hallucinations in a controlled manner. Moreover, during fine-tuning, directly applying DPO may cause the model to overly prioritize language-specific preferences, which potentially leads to suboptimal performance and an increased propensity for hallucinations (Wang et al., 2024a).

In this paper, we propose **RE-ALIGN**, a novel framework that alleviates VLM hallucinations by integrating image retrieval with direct preference optimization (DPO). Our method deliberately injects controlled hallucinations into chosen responses using image retrieval, generating rejected responses that offer more plausible and natural preference signals regarding hallucinations. Additionally, by incorporating both the retrieved image and the original input image, RE-ALIGN constructs a dual preference dataset. This dataset is then leveraged to finetune VLMs with our proposed **rdPO** objective—an extension of DPO that includes an additional visual preference optimization objective, further enhancing the alignment process with valuable visual preference signals.

2 Preliminaries

To mitigate hallucinations in VLMs, we introduce an alignment framework based on direct preference optimization (DPO) with image retrieval. In this section, we present preliminary definitions and notations for VLMs and preference optimization,

which serve as the foundation for our proposed framework.

Vision Language Models VLMs typically consist of three main components: a vision encoder $f_v(\cdot)$, a projector $f_p(\cdot)$, and an LLM backbone $\mathcal{L}(\cdot)$. Given a multimodal input query (x, v) , where x is a textual instruction and v is a visual image, VLMs generate a corresponding response $y = [y_1, \dots, y_m]$ autoregressively. Here, each y_i represents an output token, and m denotes the total number of tokens in the generated response.

Direct Preference Learning Reinforcement Learning from Human Feedback (RLHF) (Christiano et al., 2017; Ziegler et al., 2019) is a key approach for aligning machine learning models with human preferences. Among these techniques, the Direct Preference Optimization (DPO) algorithm (Rafailov et al., 2024) stands out for its popularity and for demonstrating superior alignment performance. We represent a VLM with a policy π , which, given an input query (x, v) , generates a response y from the distribution $\pi(\cdot|x, v)$. We denote by π_0 the initial VLM model, fine-tuned on instruction-following VQA data by supervised fine-tuning (SFT). Specifically, we define a preference dataset $\mathcal{D} = \{(x, v, y_w, y_l)\}$, where for each input, the response y_w is preferred to the response y_l . The DPO objective is formulated as follows, leveraging the preference dataset \mathcal{D} :

$$\mathcal{L}_{\text{DPO}} = -\mathbb{E}_{(x, v, y_w, y_l) \sim \mathcal{D}} \left[\log \sigma \left(\beta \log \frac{\pi_\theta(y_w|x, v)}{\pi_0(y_w|x, v)} - \beta \log \frac{\pi_\theta(y_l|x, v)}{\pi_0(y_l|x, v)} \right) \right].$$

Compared to deep RL-based methods like Proximal Policy Optimization (PPO) (Schulman et al., 2017; Christiano et al., 2017; Ziegler et al., 2019), DPO is more computationally efficient, easier to tune, and thus more widely adopted (Dong et al., 2024).

Image Retrieval Image retrieval aims to find relevant images from large databases – such as vector databases or indexed corpora – based on semantic similarity criteria. In this paper, we convert all images into vector representations and utilize the cosine similarity metric to evaluate their proximity to a reference image. The similarity between two images, v_1 and v_2 , is computed as follows:

$$s = \left\langle \frac{f_p(v_1)}{\|f_p(v_1)\|}, \frac{f_p(v_2)}{\|f_p(v_2)\|} \right\rangle,$$

where $\langle \cdot, \cdot \rangle$ denotes the inner product in l_2 space, $f_p(v_i)$ represents the image embeddings generated by the vision encoder $f_v(\cdot)$ of VLMs. In this paper, we employ the FAISS library (Douze et al., 2024; Johnson et al., 2019) for efficient vector searches, retrieving the top- k most relevant images.

3 Methods

In this paper, we propose RE-ALIGN, a novel framework that integrates preference optimization with image retrieval to improve cross-modal alignment in VLMs. As shown in Figure 2, the process

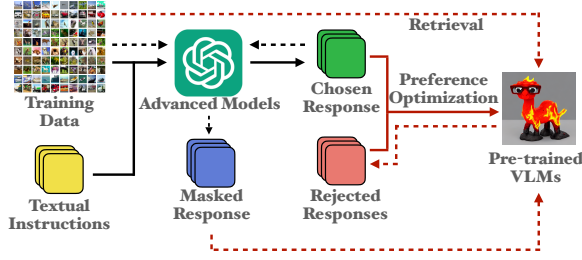


Figure 2: Illustration of RE-ALIGN framework.

begins with an advanced VLM generating chosen responses from input images from the training set. A selective masking process is then applied, strategically omitting segments associated with objects, attributes, or logical relationships identified in the image. Next, leveraging the retrieved image from the same training dataset and the masked responses, the hallucination-prone VLM is prompted to complete the masked elements, obtaining rejected responses. The generated preference pairs (chosen vs. rejected) are then used to fine-tune the VLM with $\mathcal{L}_{\text{rDPO}}$ (eq. (1)), a preference objective that integrates both visual and textual information to penalize hallucinations and reinforce grounded reasoning. Algorithm 1 in Appendix A provides an overview of RE-ALIGN, while the detailed process is explained in the following subsections.

3.1 Preference Generation

Generating high-quality preference data, which includes both accurate ground-truth responses and controlled hallucinated examples, is crucial for effective preference optimization in pre-trained VLMs. Existing methods construct preference data by perturbing ground-truth responses (Zhou et al., 2024a), corrupting visual inputs/embeddings (Deng et al., 2024; Amirloo et al., 2024) to create rejected responses, or refining responses to obtain chosen responses (Chen et al.,

2024; Yu et al., 2023a). Refinement produces high-quality preference data but comes at a high cost, whereas direct corruption is more scalable yet tends to generate unrealistic hallucinations and fails to produce plausible, natural ones in a controlled manner. To address these limitations, we introduce a novel image retrieval-based pipeline for preference data construction as shown in Figure 3, which consists of three key stages:

- **Strategical masking:** Given an input pair (x_i, v_i) and its corresponding chosen response y_w generated by a pretrained VLM, a strategic masking process removes words or segments associated with objects, attributes, or logical relationships inferred from the image, producing the masked response y_m .
- **Image retrieval:** All images $\{v_i\}$ in the training set are embedded using the original vision encoder of the pre-trained VLMs, forming the knowledge base \mathcal{K} . The top- k most similar images to v_i are then retrieved from \mathcal{K} using a cosine similarity search.
- **Inducing hallucinations:** VLMs are prompted to generate a candidate completion y_m for the masked response conditioned on the instruction x and a retrieved image v_{j_t} where $t \in [1, k]$ denotes the rank of images based on their cosine similarity to the input v_i . Both the chosen response y_w and the reconstructed response y_c are embedded using a SentenceTransformer model. If the cosine similarity between these embeddings falls below 0.95, y_c is designated as the rejected response y_l . Otherwise, the process continues with the next image $v_{j_{t+1}}$ in the similarity-ranked sequence until a suitable candidate is identified or all k retrieved images have been examined.

3.2 Preference Optimization

The curated preference dataset is subsequently used to fine-tune VLMs through direct preference learning. We propose retrieval-augmented direct preference optimization (rDPO), an extension of DPO that integrates an additional visual preference optimization objective. Given a preference dataset $\mathcal{D} = \{x, v, v_l, y_w, y_l\}$, the retrieval-augmented direct preference optimization objective is formulated as follows:

$$\mathcal{L}_{\text{vDPO}} = -\mathbb{E}_{(x,v,v_l,y_w,y_l) \sim \mathcal{D}} \left[\log \sigma \left(\beta \log \frac{\pi_{\theta}(y_w|x, v)}{\pi_0(y_w|x, v)} - \beta \log \frac{\pi_{\theta}(y_l|x, v_l)}{\pi_0(y_l|x, v_l)} \right) \right],$$

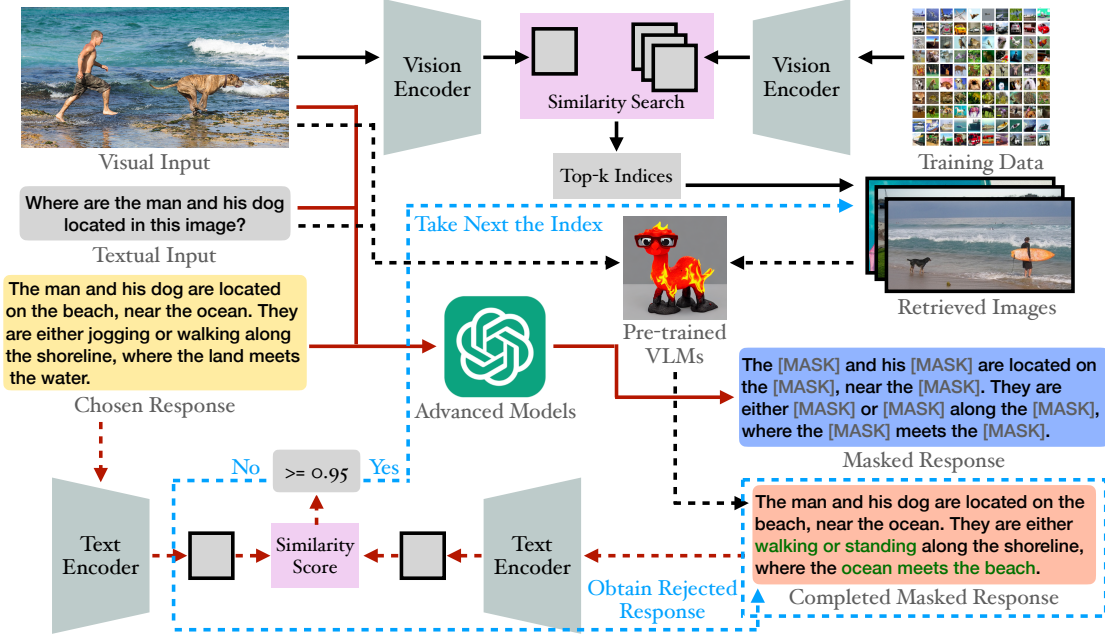


Figure 3: Illustration of the preference generation process, utilizing the original vision encoder from initial VLMs and the SentenceTransformer as the text encoder.

where (x, v) denotes the input query of VLMs, (y_w, y_l) represents the preference responses pair, and v_l is the retrieved image for v . The loss function of rDPO is the combination of standard DPO objective and visual preference optimization:

$$\mathcal{L}_{\text{rDPO}} = \mathcal{L}_{\text{DPO}} + \mathcal{L}_{\text{vDPO}}. \quad (1)$$

By incorporating both textual and visual preference signals, our approach allows VLMs to effectively exploit multimodal information during optimization, in contrast to prior alignment methods that depend exclusively on language-based preferences. In contrast to mDPO (Wang et al., 2024a), which introduces image preference by randomly cropping the original input images, rDPO adopts retrieval-augmented generation to integrate visual preference signals in a more coherent and semantically meaningful way.

4 Experiments

We conduct three categories of experiments to empirically validate the effectiveness of our proposed method. First, we evaluate the ability of RE-ALIGN to mitigate hallucinations and improve generalizability across diverse VQA tasks, demonstrating its consistent superiority over baseline approaches and achieving state-of-the-art performance. Next, we examine RE-ALIGN’s effectiveness in aligning VLMs across various model sizes and architectures, including both text-to-image and unified

models, where it delivers substantial performance over vanilla models and existing baselines. Finally, we assess the impact of our proposed rDPO objective in preference optimization, showing that it consistently surpasses standard DPO in aligning VLMs and achieving superior results in both hallucination mitigation and general tasks.

4.1 RE-ALIGN for VLMs Alignment

Datasets We conducted experiments on both hallucination detection and general VQA tasks. Specifically, we assess our method’s performance in hallucination detection using the POPE dataset (Li et al., 2023c) and Hallusion-Bench (Guan et al., 2023). For general VQA tasks, we leverage a diverse suite of benchmarks including ScienceQA (Lu et al., 2022), TextVQA (Singh et al., 2019), MM-Vet (Yu et al., 2023b), VisWiz (Gurari et al., 2018), LLaVABench (Liu, 2023), MME (Fu et al., 2023), and MMBench (Liu et al., 2024c).

Beslines We compare our method with several widely adopted alignment frameworks for VLMs, including LLaVA-RLHF (Sun et al., 2023), POVID (Zhou et al., 2024a), CSR (Zhou et al., 2024b), SIMA (Wang et al., 2024c), STIC (Deng et al., 2024). For more details on these baselines, please refer to the Appendix.

Experimental Setup We sample 11k images from the LLaVA-Instruct-150K dataset (Liu et al.,

Methods	POPE ^r	POPE ^p	POPE ^a	Hallusion ^q	Hallusion ^f	Hallusion ^{Easy}	Hallusion ^{Hard}	Hallusion ^a
LLaVA-v1.5-7B	88.14	87.23	85.10	10.3297	18.2081	41.7582	40.2326	46.3242
w. LLaVA-RLHF	84.77	84.60	83.40	10.2859	18.7861	38.2418	40.6744	44.6528
w. POVID	88.21	87.16	85.06	10.5495	18.2081	41.5385	40.9302	46.6785
w. CSR (3Iter)	87.83	87.00	85.00	10.1099	18.2081	41.7582	40.6977	46.9442
w. SIMA	88.10	87.10	85.03	10.9890	17.6301	43.0549	40.2326	45.2728
w. mDPO	88.17	87.13	85.03	9.8901	18.4971	41.978	40.000	46.1470
w. RE-ALIGN	88.65	87.43	85.16	11.2088	18.7861	45.5165	41.6279	47.6156
LLaVA-v1.6-Mistral-7B	88.83	87.93	86.43	13.6264	19.0751	47.4725	33.4884	46.0585
w. STIC	89.03	88.20	86.56	12.9670	17.3410	47.2527	34.1860	46.3242
w. RE-ALIGN	90.55	89.20	87.03	13.8462	19.0751	48.3516	34.8837	46.5899

Table 1: Impact of RE-ALIGN across hallucination benchmarks for VLMs, and comparisons with baselines.

Methods	SQA	TextVQA	MM-Vet	VisWiz	LLaVABench	MME ^P	MME ^C	MMBench	Avg. Rank
LLaVA-v1.5-7B	66.02	58.18	31.6	50.03	64.1	1510.28	357.85	64.60	3.875
w. LLaVA-RLHF	63.11	56.89	31.8	49.57	60.2	1378.90	282.85	64.39	6
w. POVID	65.98	58.18	31.8	49.80	67.3	1495.91	356.07	64.34	4.375
w. CSR (3Iter)	65.46	57.86	31.6	47.02	68.3	1525.44	365.35	64.08	4.5
w. SIMA	65.83	58.48	32.0	50.04	66.9	1510.33	371.78	64.60	2.75
w. mDPO	67.53	57.90	31.3	50.04	59.0	1510.74	335.71	64.60	4.25
w. RE-ALIGN	68.10	58.55	32.1	50.06	67.7	1511.79	367.50	64.69	1.375
LLaVA-v1.6-Mistral-7B	76.02	63.80	47.6	59.85	80.2	1494.22	323.92	69.33	2.125
w. STIC	76.42	63.50	47.3	54.21	81.0	1504.91	308.21	69.16	2.625
w. RE-ALIGN	76.47	64.08	48.3	57.27	81.8	1512.09	318.93	69.42	1.25

Table 2: Impact of RE-ALIGN across general benchmarks for VLMs, and comparisons with baselines.

2024a) to construct preference data, as illustrated in Figure 3. These images are initially used to generate QA pairs based on image captions and simple VQA tasks using GPT-4o mini (OpenAI, 2024). Furthermore, the images are encoded using clip-vit-large-patch14 (Radford et al., 2021a) to construct the knowledge base for image retrieval. For rejected responses, we use GPT-4o mini to mask the chosen response and all-mpnet-base-v2 (Reimers and Gurevych, 2019) to compute the similarity between the completed masked response and the original chosen response. We use LLaVA-v1.5-7B (Liu et al., 2024a) and LLaVA-v1.6-Mistral-7B (Li et al., 2024b) as our backbone models and perform RE-ALIGN fine-tuning for 1 epoch. All evaluations are conducted with a temperature setting of 0, and baseline results are reproduced using open-sourced model weights.

Results Table 1 shows the performance of RE-ALIGN compared to baseline methods on hallucination benchmarks. Notably, RE-ALIGN achieves the best among the evaluated methods on both POPE and HallusionBench for LLaVA-v1.5-7B (Liu et al., 2024a) and LLaVA-v1.6-Mistral-7B (Li et al., 2024b), highlighting the effectiveness of our ap-

proach in mitigating hallucinations of VLMs. As shown in Table 2, RE-ALIGN can provide generally on-par or better performance than the vanilla models and baseline alignment methods on each evaluated general VQA task, ultimately achieving the best overall results. This finding indicates that RE-ALIGN can enhance hallucination mitigation without compromising general performance.

4.2 Scalability and Generalizability

Experimental Setup The experimental setup follows the same setting as VLMs alignment experiments, except for the backbone models, where we employ a diverse array of VLMs varying in size and architecture:

- **Image-to-Text models:** the typical architecture of VLMs, where a vision encoder is integrated with an LLM to enable cross-modal understanding. In this section, we evaluate RE-ALIGN on LLaVA-v1.5-7B (Liu et al., 2024a), LLaVA-v1.5-13B (Liu et al., 2024a), LLaVA-v1.6-Vicuna-7B (Li et al., 2024b), and LLaVA-v1.6-Vicuna-13B (Li et al., 2024b).
- **Unified Models:** encoder-decoder architecture that decouples visual encoding for multimodal understanding and generation. We evaluate RE-

ALIGN on Janus-Pro-1B (Chen et al., 2025) and Janus-Pro-7B (Chen et al., 2025).

Methods	POPE ^r	POPE ^p	POPE ^a
Janus-Pro-1B	85.46	85.03	84.13
w. RE-ALIGN	87.53\uparrow2.07	87.33\uparrow2.30	85.86\uparrow1.73
Janus-Pro-7B	88.41	87.30	85.70
w. RE-ALIGN	89.73\uparrow1.32	88.37\uparrow1.07	86.27\uparrow0.57
LLaVA-v1.5-7B	88.14	87.23	85.10
w. LLaVA-RLHF	84.77\downarrow3.37	84.60\downarrow2.63	83.40\downarrow0.50
w. POVID	88.21\uparrow0.07	87.16\downarrow0.07	85.06\downarrow0.04
w. CSR (3Iter)	87.83\downarrow0.31	87.00\downarrow0.23	85.00\downarrow0.10
w. SIMA	88.10\downarrow0.04	87.10\downarrow0.13	85.03\downarrow0.07
w. mDPO	88.17\uparrow0.03	87.13\downarrow0.10	85.03\downarrow0.07
w. RE-ALIGN	88.65\uparrow0.51	87.43\uparrow0.20	85.16\uparrow0.06
LLaVA-v1.5-13B	88.07	87.53	85.60
w. CSR (3Iter)	88.38\uparrow0.31	87.90\uparrow0.37	85.46\downarrow0.14
w. SIMA	88.04\downarrow0.03	87.40\downarrow0.13	85.40\downarrow0.20
w. HSA-DPO	85.01\downarrow3.06	85.00\downarrow2.53	83.86\downarrow1.74
w. RE-ALIGN	90.03\uparrow1.96	89.20\uparrow1.30	86.20\uparrow0.74
LLaVA-v1.6-Vicuna-7B	88.52	87.63	86.36
w. RE-ALIGN	88.94\uparrow0.42	88.03\uparrow0.40	86.63\uparrow0.27
LLaVA-v1.6-Vicuna-13B	88.24	87.70	86.43
w. RE-ALIGN	88.79\uparrow0.55	88.10\uparrow0.40	86.60\uparrow0.17

Table 3: Impact of RE-ALIGN across various model scales on POPE.

Results Table 3 presents the performance of RE-ALIGN using both standard image-to-text and unified VLM backbones across model sizes from 1B to 13B on the POPE benchmark (Li et al., 2023c). In experiments with the LLaVA-v1.5 series (Liu et al., 2024a), none of the baseline approaches consistently improve performance for either the 7B or the 13B models, highlighting the limited scalability of these methods. In contrast, RE-ALIGN achieved substantial performance gains, outperforming both the baseline models and the vanilla version—most notably on the LLaVA-v1.5-13B variant. Similarly, experiments with the LLaVA-v1.6-Vicuna series (Li et al., 2024b) revealed the same trend, further underscoring RE-ALIGN’s superior scalability. For unified vision-language models, especially Janus-Pro, integrating RE-ALIGN yields a significant performance boost. Notably, Janus-Pro-1B experiences the greatest improvement, underscoring RE-ALIGN’s robustness across different model architectures. However, Janus-Pro-1B, being the smallest among the evaluated VLMs, also exhibits the poorest overall performance on POPE, suggesting a correlation between model size and the propensity for hallucinations.

4.3 Ablation Study

In this section, we conduct a comprehensive ablation study to explore how the data curation framework and design of the objective function affect the RE-ALIGN’s performance. The experimental setup follows the same setting as VLMs alignment experiments.

Dataset Due to budget constraints and the need for reproducibility, we have excluded benchmarks that require evaluation by GPT-4 (Achiam et al., 2023). Instead, we focus on the following tasks: ScienceQA (Lu et al., 2022), TextVQA (Singh et al., 2019), and POPE (Li et al., 2023c).

τ	SQA	TextVQA	POPE ^r	POPE ^p	POPE ^a
0.85	67.04	57.31	88.96	87.83	85.06
0.90	67.75	57.68	88.83	87.66	84.93
0.95	68.10	58.55	88.65	87.43	85.16

Table 4: Impact of similarity threshold τ for generating the rejected responses in RE-ALIGN across general and hallucination benchmarks for VLMs, and comparisons with baselines.

Similarity Threshold τ In RE-ALIGN, we set the similarity threshold τ to 0.95, which acts as an upper bound on the cosine similarity between the chosen response and the generated rejected response. As illustrated in Table 4, decreasing the threshold τ results in a stronger preference signal, leading to improved performance in mitigating hallucinations. However, this comes at the cost of reduced performance in general VQA. Among the evaluated configurations, setting $\tau = 0.95$ offers the best trade-off, effectively reducing hallucinations while maintaining strong performance across VQA benchmarks.

Masking Strategy In data curation, we generate preference data by inducing hallucinations at the segment level. To further investigate the impact of finer-grained perturbations, we conduct experiments using sentence-level masking. As shown in Table 5, using a sentence-level masking strategy, RE-ALIGN still demonstrates significant improvement in reducing hallucination in VLMs. However, this approach leads to a slight drop in performance on general VQA tasks. More discussions on the masking strategy can be found in Appendix F.

Design of Loss Function In RE-ALIGN, we assign equal weights to the DPO and vDPO objectives in the combined loss function, i.e., $\mathcal{L}_{\text{rDPO}} =$

Masking Strategy	SQA	TextVQA	POPE ^r	POPE ^p	POPE ^a
<i>sentence-level</i>	67.58	57.77	88.56	87.60	84.90
<i>segment-level</i>	68.10	58.55	88.65	87.43	85.16

Table 5: Impact of masking strategy across general and hallucination benchmarks for VLMs, and comparisons with baselines.

$\mathcal{L}_{\text{DPO}} + \mathcal{L}_{\text{vDPO}}$. To better understand the impact of this design of loss function, we generalize the loss function to $\mathcal{L}_{\text{DPO}} + w_v \mathcal{L}_{\text{vDPO}}$, where w_v controls the contribution of the visual component, and conduct experiments with different values of w_v to analyze the trade-offs and identify the optimal balance between textual and visual preference signals. As shown in Table 6, incorporating the $\mathcal{L}_{\text{vDPO}}$ objective significantly enhances VLM performance on hallucination benchmarks. In general, when combined with the standard \mathcal{L}_{DPO} objective, increasing the weight of $\mathcal{L}_{\text{vDPO}}$ tends to yield better overall performance. Notably, the equally-combined objective $\mathcal{L}_{\text{rDPO}}$ achieves the best balance between reducing hallucinations and maintaining strong performance on general VQA benchmarks, highlighting its effectiveness as a robust training strategy.

w_v	SQA	TextVQA	POPE ^r	POPE ^p	POPE ^a
0.0 (DPO)	66.26	58.24	88.18	87.30	85.23
0.25	67.08	58.34	88.93	87.53	84.90
0.50	67.08	58.34	88.93	87.53	84.90
0.75	67.08	58.34	88.93	87.53	84.90
1.0 (rDPO)	68.10	58.55	88.65	87.43	85.16

Table 6: Impact of rDPO objective across general and hallucination benchmarks for VLMs, and comparisons with baselines.

Results Table 6 summarizes the performance of RE-ALIGN when using both standard DPO and rDPO as the direct optimization objectives, evaluated on general VQA and hallucination tasks with LLaVA-v1.5-7B (Liu et al., 2024a) and LLaVA-v1.6-Mistral-7B (Li et al., 2024b) as backbones. The results indicate that employing rDPO as the finetuning objective consistently yields superior performance over standard DPO across both task categories, highlighting the benefits of incorporating visual preference signals during the alignment process for VLMs. Notably, even when solely employing DPO, RE-ALIGN not only achieves performance gains over the vanilla models but also outperforms the baselines evaluated in the VLM alignment experiments on several tasks. This un-

derscores the effectiveness of our image retrieval-based preference data construction.

5 Discussions

Role of Image v_l v_l is one of the top-10 retrieved images corresponding to the original image v , and qualitatively, the images v and v_l are semantically similar in terms of scenes, objects, and composition. This retrieval strategy is intended to ensure that v_l shares sufficient visual context with v , making it a plausible alternative grounding for the instruction x . Furthermore, we compute the cosine similarity between the CLIP embeddings of the caption of v (by prompting "Describe this image in detail.") and three types of images: the original image v , a retrieved image v_l , and a randomly selected image v_r . The average cosine similarities are 0.2780, 0.2382, 0.0688, respectively, which indicates that v_l retains significant semantic similarity with v and is far more aligned than an unrelated image v_r . Based on this, we interpret v_l as a "rejected input image" to the original instruction x : it provides a visually plausible but suboptimal context, under which the response y_w should be less preferred compared to when conditioned on v .

Discussion with mDPO In this section, we detail the differences between our proposed rDPO and mDPO (Wang et al., 2024a). In mDPO, a conditional preference optimization objective is introduced to force the model to determine the preference label based on visual information:

$$\mathcal{L}_{\text{CoDPO}} = -\mathbb{E}_{(x,v,y_w,y_l) \sim \mathcal{D}} \left[\log \sigma \left(\beta \log \frac{\pi_\theta(y_w|x,v)}{\pi_0(y_w|x,v)} - \beta \log \frac{\pi_\theta(y_w|x,v_c)}{\pi_0(y_w|x,v_c)} \right) \right],$$

where v_c denotes a randomly cropped image of the original input image v . Specifically, visual preference signals are generated by randomly masking 20% of the input visual tokens to encourage the model to capture preferences based on visual cues.

In contrast, RE-ALIGN extends and enhances this approach by incorporating a more semantically meaningful visual preference pair. Instead of relying solely on random crops, RE-ALIGN retrieves a relevant image from the same dataset that corresponds to the original input. This retrieval-based augmentation provides a stronger contrastive signal, improving the model’s ability to discern fine-grained visual details and reducing spurious correlations. Moreover, beyond mitigating hallucinations in VLMs, RE-ALIGN has been demonstrated

that it also significantly enhance performance on general VQA tasks.

6 Related Work

Reinforcement Learning from Human Feedback

Reinforcement Learning from Human Feedback (RLHF) has emerged as a crucial technique for incorporating human preference signals into machine learning methods and models (Dong et al., 2024). RLHF frameworks can be broadly categorized into deep RL-based approaches and direct preference learning approaches. In deep RL-based methods, a reward model is first constructed, after which Proximal Policy Optimization (PPO) (Schulman et al., 2017; Christiano et al., 2017; Ziegler et al., 2019) is employed to optimize the reward signals with KL regularization (Ouyang et al., 2022; Touvron et al., 2023b). While the direct preference learning approaches optimize a designed loss target on the offline preference dataset directly, eliminating the need for a separate reward model (Rafailov et al., 2024; Azar et al., 2024; Tang et al., 2024; Ethayarajh et al., 2024).

Vision Language Models Large Vision Language Models (VLMs) (Li et al., 2022, 2023a; Liu et al., 2024a; Li et al., 2024b; Meta, 2024; Bai et al., 2023; Wang et al., 2024b; Lu et al., 2024; Wu et al., 2024) extended the understanding and reasoning capabilities of Large Language Models (LLMs) (Devlin et al., 2018; Radford et al., 2019; Brown et al., 2020; Team et al., 2023; Roziere et al., 2023; Touvron et al., 2023a,b; Raffel et al., 2020; Yang et al., 2024; Team, 2024; Pan et al., 2023) into the visual domain. By integrating vision encoders, such as CLIP (Radford et al., 2021b), image patches are first converted into embeddings and then projected to align with text embedding space, unlocking unprecedented cross-modal applications in the real world, such as biomedical imaging (Moor et al., 2023; Li et al., 2024a), autonomous systems (Shao et al., 2024; Tian et al., 2024; Sima et al., 2023; Xing et al., 2024b; Ma et al., 2025; Wang et al., 2025), and robotics (Rana et al., 2023; Kim et al., 2024; Xing et al., 2025).

Alignment of Vision Language Models Current VLMs often suffer from hallucinations, producing inaccurate or misleading information that fails to accurately represent the content of the provided image (Zhu et al., 2024; Bai et al., 2024; Qian et al., 2025). Such misalignments can have catas-

trophic consequences when these models are deployed in real-world scenarios (Xing et al., 2024a). To address cross-modality hallucinations, recent research has primarily focused on applying direct preference optimization (Deng et al., 2024; Zhou et al., 2024a; Fang et al., 2024; Zhou et al., 2024b; Guo et al., 2024; Chen et al., 2024; Wang et al., 2024c; Yu et al., 2024b; Li et al., 2023b; Wang et al., 2024a) or contrastive learning (Sarkar et al., 2024) on the curated datasets with preference signals, and utilizing model editing techniques (Liu et al., 2024b; Yu et al., 2024a).

7 Conclusion

In this paper, a novel framework, RE-ALIGN, for aligning VLMs to mitigate hallucinations is proposed. Our approach leverages image retrieval to deliberately induce segment-level hallucinations, thereby generating plausible and natural preference signals. By integrating the retrieved images, a dual-preference dataset that encompasses both textual and visual cues is curated. Furthermore, we propose the rDPO objective, an extension of DPO that includes an additional visual preference optimization objective, to enhance the alignment process with valuable visual preference signals. Comprehensive empirical results from a range of general VQA and hallucination benchmarks demonstrate that RE-ALIGN effectively reduces hallucinations in VLMs while enhancing their overall performance. Moreover, it demonstrates superior scalability across various model architectures and sizes.

Limitations

Although RE-ALIGN has demonstrated superior performance on both hallucination and general VQA benchmarks, it does not always achieve state-of-the-art results on general tasks; in some cases, its performance is even worse than that of vanilla VLMs. Future research could explore strategies to eliminate this alignment tax or identify an optimal balance for this trade-off. The potential risks of this work align with the general challenges of RLHF alignment. As more powerful alignment techniques are developed, they may inadvertently empower adversarial approaches that exploit these models, potentially leading to unfair or discriminatory outputs. Meanwhile, these adversarial strategies can be used to generate negative samples, which can ultimately contribute to the development of more robust and reliable VLMs over time.

References

- Josh Achiam, Steven Adler, Sandhini Agarwal, Lama Ahmad, Ilge Akkaya, Florencia Leoni Aleman, Diogo Almeida, Janko Altschmidt, Sam Altman, Shyamal Anadkat, et al. 2023. Gpt-4 technical report. *arXiv preprint arXiv:2303.08774*.
- Elmira Amirloo, Jean-Philippe Fauconnier, Christoph Roesmann, Christian Kerl, Rinu Boney, Yusu Qian, Zirui Wang, Afshin Dehghan, Yinfei Yang, Zhe Gan, et al. 2024. Understanding alignment in multimodal llms: A comprehensive study. *arXiv preprint arXiv:2407.02477*.
- Mohammad Gheshlaghi Azar, Zhaohan Daniel Guo, Bilal Piot, Remi Munos, Mark Rowland, Michal Valko, and Daniele Calandriello. 2024. A general theoretical paradigm to understand learning from human preferences. In *International Conference on Artificial Intelligence and Statistics*, pages 4447–4455. PMLR.
- Jinze Bai, Shuai Bai, Shusheng Yang, Shijie Wang, Sinan Tan, Peng Wang, Junyang Lin, Chang Zhou, and Jingren Zhou. 2023. Qwen-vl: A versatile vision-language model for understanding, localization, text reading, and beyond. *arXiv preprint arXiv:2308.12966*.
- Zechen Bai, Pichao Wang, Tianjun Xiao, Tong He, Zongbo Han, Zheng Zhang, and Mike Zheng Shou. 2024. Hallucination of multimodal large language models: A survey. *arXiv preprint arXiv:2404.18930*.
- Tom Brown, Benjamin Mann, Nick Ryder, Melanie Subbiah, Jared D Kaplan, Prafulla Dhariwal, Arvind Neelakantan, Pranav Shyam, Girish Sastry, Amanda Askell, et al. 2020. Language models are few-shot learners. *Advances in neural information processing systems*, 33:1877–1901.
- Xiaokang Chen, Zhiyu Wu, Xingchao Liu, Zizheng Pan, Wen Liu, Zhenda Xie, Xingkai Yu, and Chong Ruan. 2025. Janus-pro: Unified multimodal understanding and generation with data and model scaling. *arXiv preprint arXiv:2501.17811*.
- Yangyi Chen, Karan Sikka, Michael Cogswell, Heng Ji, and Ajay Divakaran. 2024. Dress: Instructing large vision-language models to align and interact with humans via natural language feedback. In *Proceedings of the IEEE/CVF Conference on Computer Vision and Pattern Recognition*, pages 14239–14250.
- Paul F Christiano, Jan Leike, Tom Brown, Miljan Martic, Shane Legg, and Dario Amodei. 2017. Deep reinforcement learning from human preferences. *Advances in neural information processing systems*, 30.
- Chenhang Cui, Yiyang Zhou, Xinyu Yang, Shirley Wu, Linjun Zhang, James Zou, and Huaxiu Yao. 2023. Holistic analysis of hallucination in gpt-4v (ision): Bias and interference challenges. *arXiv preprint arXiv:2311.03287*.
- Yihe Deng, Pan Lu, Fan Yin, Ziniu Hu, Sheng Shen, James Zou, Kai-Wei Chang, and Wei Wang. 2024. Enhancing large vision language models with self-training on image comprehension. *arXiv preprint arXiv:2405.19716*.
- Jacob Devlin, Ming-Wei Chang, Kenton Lee, and Kristina Toutanova. 2018. Bert: Pre-training of deep bidirectional transformers for language understanding. *arXiv preprint arXiv:1810.04805*.
- Hanze Dong, Wei Xiong, Bo Pang, Haoxiang Wang, Han Zhao, Yingbo Zhou, Nan Jiang, Doyen Sahoo, Caiming Xiong, and Tong Zhang. 2024. Rlhf workflow: From reward modeling to online rlhf, 2024. URL <https://arxiv.org/abs/2405.07863>.
- Matthijs Douze, Alexandr Guzhva, Chengqi Deng, Jeff Johnson, Gergely Szilvasy, Pierre-Emmanuel Mazaré, Maria Lomeli, Lucas Hosseini, and Hervé Jégou. 2024. *The faiss library*.
- Kawin Ethayarajh, Winnie Xu, Niklas Muennighoff, Dan Jurafsky, and Douwe Kiela. 2024. Kto: Model alignment as prospect theoretic optimization. *arXiv preprint arXiv:2402.01306*.
- Yunhao Fang, Ligeng Zhu, Yao Lu, Yan Wang, Pavlo Molchanov, Jan Kautz, Jang Hyun Cho, Marco Pavone, Song Han, and Hongxu Yin. 2024. Vila²: Vila augmented vila. *arXiv preprint arXiv:2407.17453*.
- Chaoyou Fu, Peixian Chen, Yunhang Shen, Yulei Qin, Mengdan Zhang, Xu Lin, Jinrui Yang, Xiaowu Zheng, Ke Li, Xing Sun, Yunsheng Wu, and Rongrong Ji. 2023. *MME: A Comprehensive Evaluation Benchmark for Multimodal Large Language Models*. *arXiv*.
- Yuhan Fu, Ruobing Xie, Xingwu Sun, Zhanhui Kang, and Xirong Li. 2024. Mitigating hallucination in multimodal large language model via hallucination-targeted direct preference optimization. *arXiv preprint arXiv:2411.10436*.
- Tianrui Guan, Fuxiao Liu, Xiyang Wu, Ruiqi Xian, Zongxia Li, Xiaoyu Liu, Xijun Wang, Lichang Chen, Fulong Huang, Yaser Yacoub, et al. 2023. Hallusionbench: An advanced diagnostic suite for entangled language hallucination and visual illusion in large vision-language models. *arXiv preprint arXiv:2310.14566*.
- Shangmin Guo, Biao Zhang, Tianlin Liu, Tianqi Liu, Misha Khalman, Felipe Llinares, Alexandre Rame, Thomas Mesnard, Yao Zhao, Bilal Piot, et al. 2024. Direct language model alignment from online ai feedback. *arXiv preprint arXiv:2402.04792*.
- Danna Gurari, Qing Li, Abigale J Stangl, Anhong Guo, Chi Lin, Kristen Grauman, Jiebo Luo, and Jeffrey P Bigham. 2018. Vizwiz grand challenge: Answering visual questions from blind people. In *Proceedings of the IEEE conference on computer vision and pattern recognition*, pages 3608–3617.

715	Jeff Johnson, Matthijs Douze, and Hervé Jégou. 2019.	Haoyu Lu, Wen Liu, Bo Zhang, Bingxuan Wang, Kai	769
716	Billion-scale similarity search with GPUs. <i>IEEE</i>	Dong, Bo Liu, Jingxiang Sun, Tongzheng Ren, Zhu-	770
717	<i>Transactions on Big Data</i> , 7(3):535–547.	oshu Li, Hao Yang, et al. 2024. Deepseek-vl: towards	771
718	Moo Jin Kim, Karl Pertsch, Siddharth Karamcheti,	real-world vision-language understanding. <i>arXiv</i>	772
719	Ted Xiao, Ashwin Balakrishna, Suraj Nair, Rafael	<i>preprint arXiv:2403.05525</i> .	773
720	Rafailov, Ethan Foster, Grace Lam, Pannag San-	Pan Lu, Swaroop Mishra, Tony Xia, Liang Qiu, Kai-	774
721	keti, et al. 2024. Openvla: An open-source	Wei Chang, Song-Chun Zhu, Oyvind Taffjord, Peter	775
722	vision-language-action model. <i>arXiv preprint</i>	Clark, and Ashwin Kalyan. 2022. Learn to explain:	776
723	<i>arXiv:2406.09246</i> .	Multimodal reasoning via thought chains for science	777
724	Chunyu Li, Cliff Wong, Sheng Zhang, Naoto	question answering. In <i>The 36th Conference on Neu-</i>	778
725	Usuyama, Haotian Liu, Jianwei Yang, Tristan Nau-	<i>ral Information Processing Systems (NeurIPS)</i> .	779
726	mann, Hoifung Poon, and Jianfeng Gao. 2024a.	Yunsheng Ma, Wenqian Ye, Can Cui, Haiming Zhang,	780
727	Llava-med: Training a large language-and-vision	Shuo Xing, Fucui Ke, Jinhong Wang, Chenglin Miao,	781
728	assistant for biomedicine in one day. <i>Advances in</i>	Jintai Chen, Hamid Reza Tofighi, et al. 2025. Position:	782
729	<i>Neural Information Processing Systems</i> , 36.	Prospective of autonomous driving-multimodal llms	783
730	Feng Li, Renrui Zhang, Hao Zhang, Yuanhan Zhang,	world models embodied intelligence ai alignment and	784
731	Bo Li, Wei Li, Zejun Ma, and Chunyu Li. 2024b.	mamba. In <i>Proceedings of the Winter Conference on</i>	785
732	Llava-next-interleave: Tackling multi-image, video,	<i>Applications of Computer Vision</i> , pages 1010–1026.	786
733	and 3d in large multimodal models. <i>arXiv preprint</i>	Meta. 2024. Llama 3.2: Revolutionizing edge ai and	787
734	<i>arXiv:2407.07895</i> .	vision with open, customizable models .	788
735	Junnan Li, Dongxu Li, Silvio Savarese, and Steven Hoi.	Michael Moor, Qian Huang, Shirley Wu, Michihiro	789
736	2023a. Blip-2: Bootstrapping language-image pre-	Yasunaga, Yash Dalmia, Jure Leskovec, Cyril Za-	790
737	training with frozen image encoders and large lan-	kka, Eduardo Pontes Reis, and Pranav Rajpurkar.	791
738	guage models. In <i>International conference on ma-</i>	2023. Med-flamingo: a multimodal medical few-shot	792
739	<i>chine learning</i> , pages 19730–19742. PMLR.	learner. In <i>Machine Learning for Health (ML4H)</i> ,	793
740	Junnan Li, Dongxu Li, Caiming Xiong, and Steven	pages 353–367. PMLR.	794
741	Hoi. 2022. Blip: Bootstrapping language-image pre-	OpenAI. 2023. Gpt-4v(ision) system card .	795
742	training for unified vision-language understanding	OpenAI. 2024. Gpt-4o mini: advancing cost-efficient	796
743	and generation. In <i>International conference on ma-</i>	intelligence .	797
744	<i>chine learning</i> , pages 12888–12900. PMLR.	Long Ouyang, Jeffrey Wu, Xu Jiang, Diogo Almeida,	798
745	Lei Li, Zhihui Xie, Mukai Li, Shunian Chen, Peiyi	Carroll Wainwright, Pamela Mishkin, Chong Zhang,	799
746	Wang, Liang Chen, Yazheng Yang, Benyou Wang,	Sandhini Agarwal, Katarina Slama, Alex Ray, et al.	800
747	and Lingpeng Kong. 2023b. Silk: Preference dis-	2022. Training language models to follow instruc-	801
748	tillation for large visual language models. <i>arXiv</i>	tions with human feedback. <i>Advances in neural in-</i>	802
749	<i>preprint arXiv:2312.10665</i> .	<i>formation processing systems</i> , 35:27730–27744.	803
750	Yifan Li, Yifan Du, Kun Zhou, Jinpeng Wang,	Rui Pan, Shuo Xing, Shizhe Diao, Wenhe Sun, Xiang	804
751	Wayne Xin Zhao, and Ji-Rong Wen. 2023c. Eval-	Liu, Kashun Shum, Renjie Pi, Jipeng Zhang, and	805
752	uating object hallucination in large vision-language	Tong Zhang. 2023. Plum: Prompt learning using	806
753	models. <i>arXiv preprint arXiv:2305.10355</i> .	metaheuristic. <i>arXiv preprint arXiv:2311.08364</i> .	807
754	Haotian Liu. 2023. Llava-bench .	Chengxuan Qian, Shuo Xing, Shawn Li, Yue Zhao, and	808
755	Haotian Liu, Chunyu Li, Qingyang Wu, and Yong Jae	Zhengzhong Tu. 2025. Decalign: Hierarchical cross-	809
756	Lee. 2024a. Visual instruction tuning. <i>Advances in</i>	modal alignment for decoupled multimodal represen-	810
757	<i>neural information processing systems</i> , 36.	tation learning. <i>arXiv preprint arXiv:2503.11892</i> .	811
758	Shi Liu, Kecheng Zheng, and Wei Chen. 2024b. Pay-	Alec Radford, Jong Wook Kim, Chris Hallacy, Aditya	812
759	ing more attention to image: A training-free method	Ramesh, Gabriel Goh, Sandhini Agarwal, Girish Sas-	813
760	for alleviating hallucination in lvlms. In <i>European</i>	try, Amanda Askell, Pamela Mishkin, Jack Clark,	814
761	<i>Conference on Computer Vision</i> , pages 125–140.	et al. 2021a. Learning transferable visual models	815
762	Springer.	from natural language supervision. In <i>International</i>	816
763	Yuan Liu, Haodong Duan, Yuanhan Zhang, Bo Li,	<i>conference on machine learning</i> , pages 8748–8763.	817
764	Songyang Zhang, Wangbo Zhao, Yike Yuan, Jiaqi	PMLR.	818
765	Wang, Conghui He, Ziwei Liu, et al. 2024c. Mm-	Alec Radford, Jong Wook Kim, Chris Hallacy, Aditya	819
766	bench: Is your multi-modal model an all-around	Ramesh, Gabriel Goh, Sandhini Agarwal, Girish Sas-	820
767	player? In <i>European conference on computer vi-</i>	try, Amanda Askell, Pamela Mishkin, Jack Clark,	821
768	<i>sion</i> , pages 216–233. Springer.	et al. 2021b. Learning transferable visual models	822
		from natural language supervision. In <i>International</i>	823

824	<i>conference on machine learning</i> , pages 8748–8763.	Amanpreet Singh, Vivek Natarajan, Meet Shah,	879
825	PMLR.	Yu Jiang, Xinlei Chen, Dhruv Batra, Devi Parikh,	880
826	Alec Radford, Jeffrey Wu, Rewon Child, David Luan,	and Marcus Rohrbach. 2019. Towards vqa models	881
827	Dario Amodei, Ilya Sutskever, et al. 2019. Language	that can read. In <i>Proceedings of the IEEE/CVF con-</i>	882
828	models are unsupervised multitask learners. <i>OpenAI</i>	<i>ference on computer vision and pattern recognition</i> ,	883
829	<i>blog</i> , 1(8):9.	pages 8317–8326.	884
830	Rafael Rafailov, Archit Sharma, Eric Mitchell, Christo-	Zhiqing Sun, Sheng Shen, Shengcao Cao, Haotian Liu,	885
831	pher D Manning, Stefano Ermon, and Chelsea Finn.	Chunyu Li, Yikang Shen, Chuang Gan, Liang-	886
832	2024. Direct preference optimization: Your language	Yan Gui, Yu-Xiong Wang, Yiming Yang, et al. 2023.	887
833	model is secretly a reward model. <i>Advances in Neu-</i>	Aligning large multimodal models with factually aug-	888
834	<i>ral Information Processing Systems</i> , 36.	mented rlhf. <i>arXiv preprint arXiv:2309.14525</i> .	889
835	Colin Raffel, Noam Shazeer, Adam Roberts, Katherine	Yunhao Tang, Zhaohan Daniel Guo, Zeyu Zheng,	890
836	Lee, Sharan Narang, Michael Matena, Yanqi Zhou,	Daniele Calandriello, Rémi Munos, Mark Row-	891
837	Wei Li, and Peter J Liu. 2020. Exploring the lim-	land, Pierre Harvey Richemond, Michal Valko,	892
838	its of transfer learning with a unified text-to-text	Bernardo Ávila Pires, and Bilal Piot. 2024. General-	893
839	transformer. <i>Journal of machine learning research</i> ,	ized preference optimization: A unified approach to	894
840	21(140):1–67.	offline alignment. <i>arXiv preprint arXiv:2402.05749</i> .	895
841	Krishan Rana, Jesse Haviland, Sourav Garg, Jad Abou-	Gemini Team, Rohan Anil, Sebastian Borgeaud,	896
842	Chakra, Ian Reid, and Niko Suenderhauf. 2023. Say-	Yonghui Wu, Jean-Baptiste Alayrac, Jiahui Yu,	897
843	plan: Grounding large language models using 3d	Radu Soricut, Johan Schalkwyk, Andrew M Dai,	898
844	scene graphs for scalable robot task planning. In <i>7th</i>	Anja Hauth, et al. 2023. Gemini: a family of	899
845	<i>Annual Conference on Robot Learning</i> .	highly capable multimodal models. <i>arXiv preprint</i>	900
846	Nils Reimers and Iryna Gurevych. 2019. <i>Sentence-bert:</i>	<i>arXiv:2312.11805</i> .	901
847	<i>Sentence embeddings using siamese bert-networks</i> .	Qwen Team. 2024. <i>Qwen2.5: A party of foundation</i>	902
848	In <i>Proceedings of the 2019 Conference on Empirical</i>	<i>models</i> .	903
849	<i>Methods in Natural Language Processing</i> . Associa-	Xiaoyu Tian, Junru Gu, Bailin Li, Yicheng Liu, Chenxu	904
850	tion for Computational Linguistics.	Hu, Yang Wang, Kun Zhan, Peng Jia, Xianpeng Lang,	905
851	Anna Rohrbach, Lisa Anne Hendricks, Kaylee Burns,	and Hang Zhao. 2024. Drivevlm: The convergence of	906
852	Trevor Darrell, and Kate Saenko. 2018. Object	autonomous driving and large vision-language mod-	907
853	hallucination in image captioning. <i>arXiv preprint</i>	els. <i>arXiv preprint arXiv:2402.12289</i> .	908
854	<i>arXiv:1809.02156</i> .	Hugo Touvron, Thibaut Lavril, Gautier Izacard, Xavier	909
855	Baptiste Roziere, Jonas Gehring, Fabian Gloeckle, Sten	Martinet, Marie-Anne Lachaux, Timothée Lacroix,	910
856	Sootla, Itai Gat, Xiaoqing Ellen Tan, Yossi Adi,	Baptiste Rozière, Naman Goyal, Eric Hambro, Faisal	911
857	Jingyu Liu, Tal Remez, Jérémy Rapin, et al. 2023.	Azhar, et al. 2023a. Llama: Open and effi-	912
858	Code llama: Open foundation models for code. <i>arXiv</i>	cient foundation language models. <i>arXiv preprint</i>	913
859	<i>preprint arXiv:2308.12950</i> .	<i>arXiv:2302.13971</i> .	914
860	Pritam Sarkar, Sayna Ebrahimi, Ali Etemad, Ahmad	Hugo Touvron, Louis Martin, Kevin Stone, Peter Al-	915
861	Beirami, Sercan Ö Arık, and Tomas Pfister. 2024.	bert, Amjad Almahairi, Yasmine Babaei, Nikolay	916
862	Mitigating object hallucination via data augmented	Bashlykov, Soumya Batra, Prajjwal Bhargava, Shruti	917
863	contrastive tuning. <i>arXiv preprint arXiv:2405.18654</i> .	Bhosale, et al. 2023b. Llama 2: Open founda-	918
864	John Schulman, Filip Wolski, Prafulla Dhariwal,	tion and fine-tuned chat models. <i>arXiv preprint</i>	919
865	Alec Radford, and Oleg Klimov. 2017. Proxi-	<i>arXiv:2307.09288</i> .	920
866	mal policy optimization algorithms. <i>arXiv preprint</i>	Fei Wang, Wenxuan Zhou, James Y Huang, Nan Xu,	921
867	<i>arXiv:1707.06347</i> .	Sheng Zhang, Hoifung Poon, and Muhao Chen.	922
868	Hao Shao, Yuxuan Hu, Letian Wang, Guanglu Song,	2024a. mdpo: Conditional preference optimiza-	923
869	Steven L Waslander, Yu Liu, and Hongsheng Li. 2024.	tion for multimodal large language models. <i>arXiv</i>	924
870	Lmdrive: Closed-loop end-to-end driving with large	<i>preprint arXiv:2406.11839</i> .	925
871	language models. In <i>Proceedings of the IEEE/CVF</i>	Peng Wang, Shuai Bai, Sinan Tan, Shijie Wang, Zhi-	926
872	<i>Conference on Computer Vision and Pattern Recog-</i>	hao Fan, Jinze Bai, Keqin Chen, Xuejing Liu, Jialin	927
873	<i>nition</i> , pages 15120–15130.	Wang, Wenbin Ge, Yang Fan, Kai Dang, Mengfei	928
874	Chonghao Sima, Katrin Renz, Kashyap Chitta, Li Chen,	Du, Xuancheng Ren, Rui Men, Dayiheng Liu,	929
875	Hanxue Zhang, Chengen Xie, Ping Luo, Andreas	Chang Zhou, Jingren Zhou, and Junyang Lin. 2024b.	930
876	Geiger, and Hongyang Li. 2023. Drivelm: Driving	Qwen2-vl: Enhancing vision-language model’s per-	931
877	with graph visual question answering. <i>arXiv preprint</i>	ception of the world at any resolution. <i>arXiv preprint</i>	932
878	<i>arXiv:2312.14150</i> .	<i>arXiv:2409.12191</i> .	933

934	Xiyao Wang, Jiuhai Chen, Zhaoyang Wang, Yuhang	Cui, Zhenru Zhang, and Zhihao Fan. 2024. Qwen2	991
935	Zhou, Yiyang Zhou, Huaxiu Yao, Tianyi Zhou,	technical report. <i>arXiv preprint arXiv:2407.10671</i> .	992
936	Tom Goldstein, Parminder Bhatia, Furong Huang,		
937	et al. 2024c. Enhancing visual-language modality	Runpeng Yu, Weihao Yu, and Xinchao Wang. 2024a.	993
938	alignment in large vision language models via self-	Attention prompting on image for large vision-	994
939	improvement. <i>arXiv preprint arXiv:2405.15973</i> .	language models. In <i>European Conference on Com-</i>	995
		<i>puter Vision</i> , pages 251–268. Springer.	996
940	Yuping Wang, Shuo Xing, Cui Can, Renjie Li,	Tianyu Yu, Jinyi Hu, Yuan Yao, Haoye Zhang, Yue	997
941	Hongyuan Hua, Kexin Tian, Zhaobin Mo, Xiangbo	Zhao, Chongyi Wang, Shan Wang, Yinxv Pan, Jiao	998
942	Gao, Keshu Wu, Sulong Zhou, et al. 2025. Genera-	Xue, Dahai Li, et al. 2023a. Reformulating vision-	999
943	tive ai for autonomous driving: Frontiers and oppor-	language foundation models and datasets towards	1000
944	tunities. <i>arXiv preprint arXiv:2505.08854</i> .	universal multimodal assistants. <i>arXiv preprint</i>	1001
		<i>arXiv:2310.00653</i> .	1002
945	Zhiyu Wu, Xiaokang Chen, Zizheng Pan, Xingchao		
946	Liu, Wen Liu, Damai Dai, Huazuo Gao, Yiyang	Tianyu Yu, Yuan Yao, Haoye Zhang, Taiwan He, Yifeng	1003
947	Ma, Chengyue Wu, Bingxuan Wang, et al. 2024.	Han, Ganqu Cui, Jinyi Hu, Zhiyuan Liu, Hai-Tao	1004
948	Deepseek-vl2: Mixture-of-experts vision-language	Zheng, Maosong Sun, et al. 2024b. RLhf-v: Towards	1005
949	models for advanced multimodal understanding.	trustworthy mllms via behavior alignment from fine-	1006
950	<i>arXiv preprint arXiv:2412.10302</i> .	grained correctional human feedback. In <i>Proceed-</i>	1007
		<i>ings of the IEEE/CVF Conference on Computer Vi-</i>	1008
951	Wenyi Xiao, Ziwei Huang, Leilei Gan, Wanggui He,	<i>sion and Pattern Recognition</i> , pages 13807–13816.	1009
952	Haoyuan Li, Zhelun Yu, Fangxun Shu, Hao Jiang,		
953	and Linchao Zhu. 2025. Detecting and mitigating	Weihao Yu, Zhengyuan Yang, Linjie Li, Jianfeng Wang,	1010
954	hallucination in large vision language models via fine-	Kevin Lin, Zicheng Liu, Xinchao Wang, and Lijuan	1011
955	grained ai feedback. In <i>Proceedings of the AAAI Con-</i>	Wang. 2023b. Mm-vet: Evaluating large multimodal	1012
956	<i>ference on Artificial Intelligence</i> , volume 39, pages	models for integrated capabilities. <i>arXiv preprint</i>	1013
957	25543–25551.	<i>arXiv:2308.02490</i> .	1014
958	Yuxi Xie, Guanzhen Li, Xiao Xu, and Min-Yen Kan.	Yiyang Zhou, Chenhang Cui, Rafael Rafailov, Chelsea	1015
959	2024. V-dpo: Mitigating hallucination in large vision	Finn, and Huaxiu Yao. 2024a. Aligning modalities	1016
960	language models via vision-guided direct preference	in vision large language models via preference fine-	1017
961	optimization. <i>arXiv preprint arXiv:2411.02712</i> .	tuning. <i>arXiv preprint arXiv:2402.11411</i> .	1018
962	Shuo Xing, Hongyuan Hua, Xiangbo Gao, Shenzhe Zhu,	Yiyang Zhou, Zhiyuan Fan, Dongjie Cheng, Sihan Yang,	1019
963	Renjie Li, Kexin Tian, Xiaopeng Li, Heng Huang,	Zhaorun Chen, Chenhang Cui, Xiyao Wang, Yun	1020
964	Tianbao Yang, Zhangyang Wang, Yang Zhou, Huaxiu	Li, Linjun Zhang, and Huaxiu Yao. 2024b. Cali-	1021
965	Yao, and Zhengzhong Tu. 2024a. AutoTrust: Bench-	brated self-rewarding vision language models. <i>arXiv</i>	1022
966	marking Trustworthiness in Large Vision Language	<i>preprint arXiv:2405.14622</i> .	1023
967	Models for Autonomous Driving . <i>arXiv</i> .		
968	Shuo Xing, Chengyuan Qian, Yuping Wang, Hongyuan	Tinghui Zhu, Qin Liu, Fei Wang, Zhengzhong Tu,	1024
969	Hua, Kexin Tian, Yang Zhou, and Zhengzhong Tu.	and Muhao Chen. 2024. Unraveling cross-modality	1025
970	2024b. Openemmas: Open-source multimodal model	knowledge conflicts in large vision-language models.	1026
971	for end-to-end autonomous driving . <i>arXiv</i> .	<i>arXiv preprint arXiv:2410.03659</i> .	1027
972	Shuo Xing, Zezhou Sun, Shuangyu Xie, Kaiyuan Chen,	Daniel M Ziegler, Nisan Stiennon, Jeffrey Wu, Tom B	1028
973	Yanjia Huang, Yuping Wang, Jiachen Li, Dezhen	Brown, Alec Radford, Dario Amodei, Paul Chris-	1029
974	Song, and Zhengzhong Tu. 2025. Can large vision	tiano, and Geoffrey Irving. 2019. Fine-tuning lan-	1030
975	language models read maps like a human? <i>arXiv</i>	guage models from human preferences. <i>arXiv</i>	1031
976	<i>preprint arXiv:2503.14607</i> .	<i>preprint arXiv:1909.08593</i> .	1032
977	An Yang, Baosong Yang, Binyuan Hui, Bo Zheng,		
978	Bowen Yu, Chang Zhou, Chengpeng Li, Chengyuan		
979	Li, Dayiheng Liu, Fei Huang, Guanting Dong, Hao-		
980	ran Wei, Huan Lin, Jialong Tang, Jialin Wang, Jian		
981	Yang, Jianhong Tu, Jianwei Zhang, Jianxin Ma, Jin		
982	Xu, Jingren Zhou, Jinze Bai, Jinzheng He, Junyang		
983	Lin, Kai Dang, Keming Lu, Keqin Chen, Kexin Yang,		
984	Mei Li, Mingfeng Xue, Na Ni, Pei Zhang, Peng		
985	Wang, Ru Peng, Rui Men, Ruize Gao, Runji Lin,		
986	Shijie Wang, Shuai Bai, Sinan Tan, Tianhang Zhu,		
987	Tianhao Li, Tianyu Liu, Wenbin Ge, Xiaodong Deng,		
988	Xiaohuan Zhou, Xingzhang Ren, Xinyu Zhang, Xipin		
989	Wei, Xuancheng Ren, Yang Fan, Yang Yao, Yichang		
990	Zhang, Yu Wan, Yunfei Chu, Yuqiong Liu, Zeyu		

A Overview of RE-ALIGN

Algorithm 1 Overview of RE-ALIGN

Required:

- (1) Unlabeled images $\{v_i\}$ with instructions $\{x_i\}$;
- (2) an advanced VLM model \mathcal{V} ;
- (3) caption masking prompt P_m ;
- (4) masked caption completion prompt P_c ;
- (5) a text encoder \mathcal{T} .

Input: A reference model π_0 with vision encoder $f_v(\cdot)$, VLM π_θ , hyper-parameter k, τ .

```

1:  $\mathcal{D} \leftarrow \emptyset$  // Init preference dataset
2:  $N \leftarrow |\{v_i\}|$ 
3: for  $i = 1, \dots, N$  do
4:    $y_w \leftarrow \mathcal{V}(x_i, v_i)$  // Get preferred response
5:    $y_m \leftarrow \mathcal{V}(P_m, x_i, v_i)$  // Strategic masking
6:    $s_i^j = \text{sim}(f_v(v_i), f_v(v_j)), \forall i \neq j$ 
7:   // Retrieve top- $k$  similar images
8:    $s_i^{j_1}, \dots, s_i^{j_k} \leftarrow \text{Top}_k(s_i^j)$ 
9:    $y_l \leftarrow \text{None}, v_l \leftarrow \text{None}$ 
10:  for  $t = 1, \dots, k$  do
11:    // Generate candidate hallucinations
12:     $y_c \leftarrow \mathcal{V}(P_c, y_m, v_{j_t})$ 
13:    if  $\text{sim}(\mathcal{T}(y_w), \mathcal{T}(y_c)) \geq \tau$  then
14:      // Assign rejected response
15:       $y_l \leftarrow y_c, v_l \leftarrow v_{j_k}$ 
16:  if  $y_l$  is None then
17:    continue
18:   $\mathcal{D} \leftarrow \mathcal{D} \cup \{x_i, v_i, v_l, y_w, y_l\}$ 
19: Update  $\pi_\theta$  through  $\mathcal{L}_{\text{rDPO}}$  (eq. (1))
20: return  $\pi_\theta$ 

```

B Details of the Evaluated Baselines

We compare our proposed method with the following alignment frameworks for VLMs:

- **LLaVA-RLHF** (Sun et al., 2023): conducts SFT on for updating the projector only and then PPO on the preference data collected from human annotators.
- **POVID** (Zhou et al., 2024a): constructing preference data by prompting GPT-4V (OpenAI, 2023) to generate hallucinations while intentionally injecting noise into image inputs, followed by fine-tuning VLMs using DPO.
- **CSR** (Zhou et al., 2024b): iteratively generates candidate responses and curates preference data using a self-rewarding mechanism, followed by fine-tuning VLMs via DPO.

- **SIMA** (Wang et al., 2024c): self-generates responses and employs an in-context self-critic mechanism to select response pairs for preference data construction, followed by fine-tuning with DPO.

- **STIC** (Deng et al., 2024): self-generates chosen responses and constructs preference data by introducing corrupted images or misleading prompts, followed by fine-tuning with regularized DPO.

- **mDPO** (Wang et al., 2024a): finetunes the model with conditional preference optimization, which incorporates an additional objective to account for image-level preferences and a reward anchor that forces the reward to be positive for chosen responses.

C Prompts used for Preference Data Construction

During the construction of the preference dataset for RE-ALIGN, we employed GPT-4o mini (OpenAI, 2024) to mask the chosen response using the following prompt.

Strategic Masking

Please mask any words of the segments related to the objects, attributes, and logical relationships of the input image in the following description by replacing them with [MASK].

Then, we instruct the VLMs to produce a candidate completion for the masked response to generate the final rejected response using the following prompt.

Masking Completion

Please complete the following sentence based on the input image by filling in the masked segments.

D Examples of Preference Pair

Table 4 and 5 provide examples of the constructed preference data for the VQA and image captioning, and each data sample contains textual instruction, input image, retrieved image, chosen response, and rejected response.

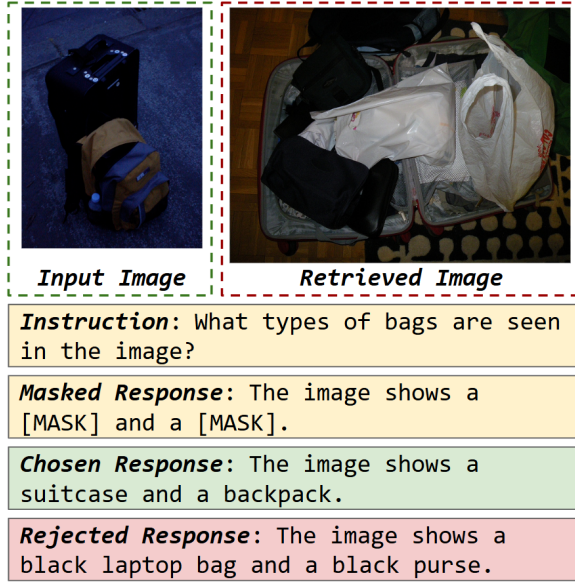


Figure 4: Example preference pair for VQA generated using RE-ALIGN.

E Response Examples

Figure 6 presents example responses from both the original LLaVA-v1.5-7B model and RE-ALIGN as evaluated on LLaVABench. Notably, the original model’s response exhibits server object hallucinations, while RE-ALIGN delivers a clearer and more accurate description of the image.

F Additional Discussions

Performance Variations on General VQA tasks

While RE-ALIGN consistently delivers the best performance on hallucination benchmarks across all backbone models, it may not achieve the top result for every general VQA benchmark. The variations in performance on general VQA tasks are primarily due to the alignment tax, a well-known phenomenon in RLHF, where alignment can sometimes lead to a decline in the model’s ability to retain pretraining knowledge. Notably, this trade-off is not unique to RE-ALIGN; as shown in Table 2, several baselines even underperform compared to the vanilla VLMs on general VQA tasks.

Segment-level Preference Building on the findings of (Yu et al., 2024b), we generate preference data by inducing hallucinations at the segment level than at the sentence level (as seen in approaches such as POVID (Zhou et al., 2024a), STIC (Deng et al., 2024), and CSR (Zhou et al., 2024b)), to provide robust supervision signals during the alignment process. This finer-grained preference model-

ing yields clearer and more precise learning signals, enabling the model to better distinguish between subtle hallucinations and ground truth responses. To further investigate these segment-level preference signals, we expanded the finetuning dataset from 11k to 16k image samples. As illustrated in Figure 7, when using LLaVA-v1.6-Mistral-7B as the backbone with ScienceQA as the case study, RE-ALIGN achieved a significant performance improvement—from 0.45 to 1.34—demonstrating the effectiveness of our approach.

G Licenses

The LLaVA-Instruct-150K dataset (Liu et al., 2024a) which is used to construct preference data is released under CC BY 4.0 license and it should abide by the policy of OpenAI¹.

For the hallucination benchmarks, POPE (Li et al., 2023c) and HallusionBench (Guan et al., 2023) are released under MIT and BSD-3-Clause licenses.

For the general VQA benchmarks, ScienceQA (Lu et al., 2022), TextVQA (Singh et al., 2019), MM-Vet (Yu et al., 2023b), VisWiz (Gurari et al., 2018), LLaVABench (Liu, 2023), and MMBench (Liu et al., 2024c) are released under MIT, CC BY 4.0, Apache-2.0, CC BY 4.0, Apache-2.0, and Apache-2.0 licenses respectively. While MME (Fu et al., 2023) was released without an accompanying license.

H Experimental Cost

The cost for curating the preference dataset by using GPT-4o mini (OpenAI, 2024) cost approximately \$90 in total. The evaluation of HallusionBench and LLaVABench using GPT-4 (Achiam et al., 2023) incurred an approximate total cost of \$30.

I Computational Cost

All finetuning and evaluation experiments were executed on four NVIDIA A6000ada GPUs. Table 7 details the time required for RE-ALIGN to finetune each model.

J Hyperparameter Setting

For all the experiments, we finetuning VLMs with RE-ALIGN for 1 epoch. We deploy LoRA finetuning with $\text{lora_r}=128$, $\text{lora_alpha}=256$,

¹<https://openai.com/policies/terms-of-use>



Figure 5: Example preference pair for image captioning generated using RE-ALIGN.

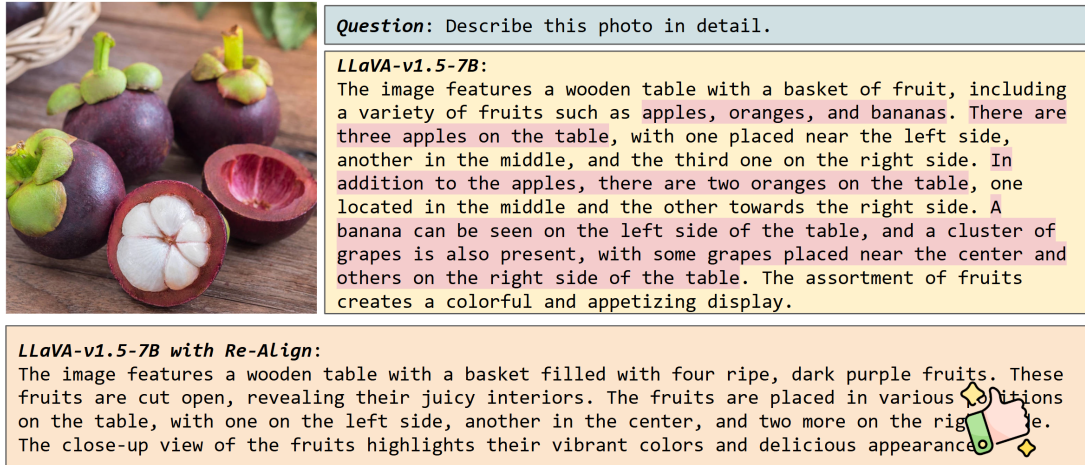


Figure 6: Example responses generated by LLaVA-v1.5-7B and RE-ALIGN.

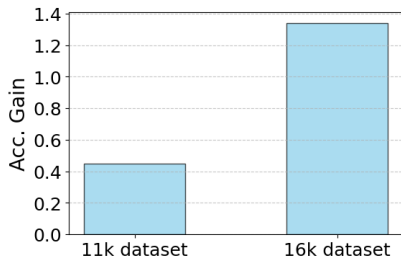


Figure 7: Performance gains of RE-ALIGN with LLaVA-v1.6-Mistral-7B as the backbone on ScienceQA with respect to the size of preference data.

Models	Required Time
Janus-Pro-1B	50 min
Janus-Pro-7B	93 min
LLaVA-v1.5-7B	35 min
LLaVA-v1.5-13B	45 min
LLaVA-v1.6-Mistral-7B	30 min
LLaVA-v1.6-Vicuna-7B	46 min
LLaVA-v1.6- Vicuna-13B	72 min

Table 7: Time required for finetuning VLMs with RE-ALIGN.

target_module=all, and hyperparameters as presented in Table 8.

Hyperparameter	Setting
β	0.1
Learning rate	1e-5
weight_decay	0.0
warmup_ratio	0.03
lr_scheduler_type	cosine
mm_projector_lr	2e-5
mm_projector_type	mlp2x_gelu
gradient_accumulation_steps	8
per_device_train_batch_size	1
bf16	True
Optimizer	AdamW

Table 8: Hypeterparameter setting for finetuning.

K Social Impacts

Our proposed novel alignment framework for VLMs, RE-ALIGN, not only significantly mitigates the hallucinations of VLMs but also elevates their generalization capabilities across diverse multimodal tasks. These advancements hold far-reaching societal implications, particularly in advancing the development of trustworthy, ethically aligned AI systems capable of reliable real-world deployment. To elucidate these implications, we provide a comprehensive overview of potential transformative outcomes:

- **Enhancing trustworthiness:** RE-ALIGN significantly enhances the reliability of AI-generated content by reducing hallucinated outputs and improving factual grounding. This ensures that users and regulatory bodies can place increased confidence in AI-driven decisions and recommendations.
- **Safety-critical applications:** By reducing erratic outputs and improving contextual awareness, RE-ALIGN enables safer deployment of VLMs in high-stakes domains such as healthcare diagnostics, autonomous vehicles, and disaster response systems, where error margins are near-zero and algorithmic trust is paramount.
- **Democratizing access to robust AI:** Our method can democratize access to advanced multimodal AI models under low-resource or data-scarce settings, which empowers researchers and practitioners with limited computational resources to participate in cutting-edge AI development, ultimately contributing to a more equitable and diverse AI ecosystem.